molecules

MDPI

Article

Photodynamic Inactivation of Bacteria and Biofilms with Benzoselenadiazole-Doped Metal-Organic Frameworks

Liang Luan [1,†], Lehan Du [2,†], Wenjun Shi [2], Yunhui Li [1,*] and Quan Zhang [2,*]

[1] Department of Laboratory Medical Center, General Hospital of Northern Theater Command, No. 83, Wenhua Road, Shenhe District, Shenyang 110016, China
[2] Institute of Smart Biomedical Materials, School of Materials Science and Engineering, Zhejiang Sci-Tech University, Hangzhou 310018, China
* Correspondence: 18909882737@163.com (Y.L.); quanzhang@zstu.edu.cn (Q.Z.)
† These authors contributed equally to this work.

Abstract: Bacterial biofilms are difficult to treat due to their resistance to traditional antibiotics. Although photodynamic therapy (PDT) has made significant progress in biomedical applications, most photosensitizers have poor water solubility and can thus aggregate in hydrophilic environments, leading to the quenching of photosensitizing activity in PDT. Herein, a benzoselenadiazole-containing ligand was designed and synthesized to construct the zirconium (IV)-based benzoselenadiazole-doped metal-organic framework (Se-MOF). Characterizations revealed that Se-MOF is a type of UiO-68 topological framework with regular crystallinity and high porosity. Compared to the MOF without benzoselenadiazole, Se-MOF exhibited a higher $^1O_2$ generation efficacy and could effectively kill *Staphylococcus aureus* bacteria under visible-light irradiation. Importantly, in vitro biofilm experiments confirmed that Se-MOF could efficiently inhibit the formation of bacteria biofilms upon visible-light exposure. This study provides a promising strategy for developing MOF-based PDT agents, facilitating their transformation into clinical photodynamic antibacterial applications.

Keywords: antimicrobial agents; bacteria; biofilms; irradiation; metal-organic frameworks

Citation: Luan, L.; Du, L.; Shi, W.; Li, Y.; Zhang, Q. Photodynamic Inactivation of Bacteria and Biofilms with Benzoselenadiazole-Doped Metal-Organic Frameworks. *Molecules* **2022**, *27*, 8908. https://doi.org/10.3390/molecules27248908

Academic Editor: Peizhou Li

Received: 15 November 2022
Accepted: 11 December 2022
Published: 14 December 2022

1. Introduction

In recent decades, bacterial resistance to antibiotics has occurred frequently due to the misuse and overuse of antibiotics, leading to a failure to treat bacterial infectious diseases [1–3]. In addition, most bacterial infections are related to the formation of biofilms. Generally, bacteria can secrete extracellular polymeric substances such as lipids, proteins, and polysaccharides and embed themselves to form a cohesive network containing multiple cells [4,5]. Compared to separated bacteria, bacterial biofilms are 10–1000 times more resistant to antibiotics [6,7]. Although numerous antibacterial agents and antiseptic techniques have been proposed, there remains a pressing need for new antibacterial reagents that are not dependent on antibiotics and can increase the efficiencies of killing pathogens resistant to antibiotics and inhibiting the formation of bacterial biofilms [8–10].

Photodynamic therapy (PDT) has been widely studied as a promising treatment strategy for bacteria ablation because it does not cause bacterial resistance to light treatment [11–13]. The PDT process begins when a photosensitizer (PS) is activated by light of the appropriate wavelength to transfer energy to molecular oxygen and produces highly cytotoxic reactive oxygen species, primarily singlet oxygen ($^1O_2$), which damages the membrane and DNA of bacterial cells and leads to cell death. To date, various organic PSs have been developed, including porphyrins [14,15], phthalocyanines [16,17], and boron dipyrromethene [18,19]. However, the use of organic PSs is often limited by their aggregation in physiological environments, leading to the loss of photosensitizing activity [20–23]. Inorganic nanomaterials can also act as PSs to kill bacteria under light irradiation but exhibit severe toxic effects on specific mammalian cells [24–26].

Metal-organic frameworks (MOFs) are a class of porous materials composed of inorganic metals and coordinating organic ligands [27–29]. Recently, MOFs have been widely explored for biomedical applications due to their unique properties, including tunable composition and size, large surface area, and high porosity for the delivery of various therapeutic agents [30–32]. When PSs are incorporated into MOF skeletons, various photosensitive MOFs have been developed for photodynamic antibacterial applications. For example, porphyrin-based MOFs have been explored in bacterial treatment, as they can avoid the self-quenching of PSs and facilitate the diffusion of $^1O_2$, thus improving the PDT efficacy of photosensitive MOFs [33–35]. Although various photosensitive MOFs have been studied for photodynamic antibacterial applications, there is still a need to develop a simple strategy for preparing photosensitive MOFs, which can effectively inhibit the formation of bacterial biofilms.

In this study, we report a strategy for preparing zirconium (IV)-based benzoselenadiazole-doped MOFs with mixed ligands and demonstrate their effectiveness for the photodynamic inactivation of bacteria and biofilms. The structure and preparation strategy of the MOFs are illustrated in Figure 1. The dimethyl-substituted dicarboxylate ligand (mTPDC-H2) was first synthesized to construct a topological UiO framework (Me-MOF). Furthermore, the benzoselenadiazole-containing ligand (SeTPDC-H2) was synthesized and mixed with mTPDC-H2 to form the benzoselenadiazole-doped MOF (Se-MOF). To endow MOFs with photodynamic properties, the introduction of selenium atoms in the Se-MOF can effectively exert the heavy-atom effect that enhances the intersystem crossing of the exciting energy. In addition, the incorporation of benzoselenadiazole-containing ligands into MOF skeletons can also avoid the aggregation of organic photosensitizers [36]. The photodynamic antibacterial activity of Me-MOF and Se-MOF against *Staphylococcus aureus* (*S. aureus*) bacteria was studied. Finally, the bacterial biofilm model was established to evaluate the inhibition effect of Me-MOF and Se-MOF on biofilm formation under visible-light irradiation.

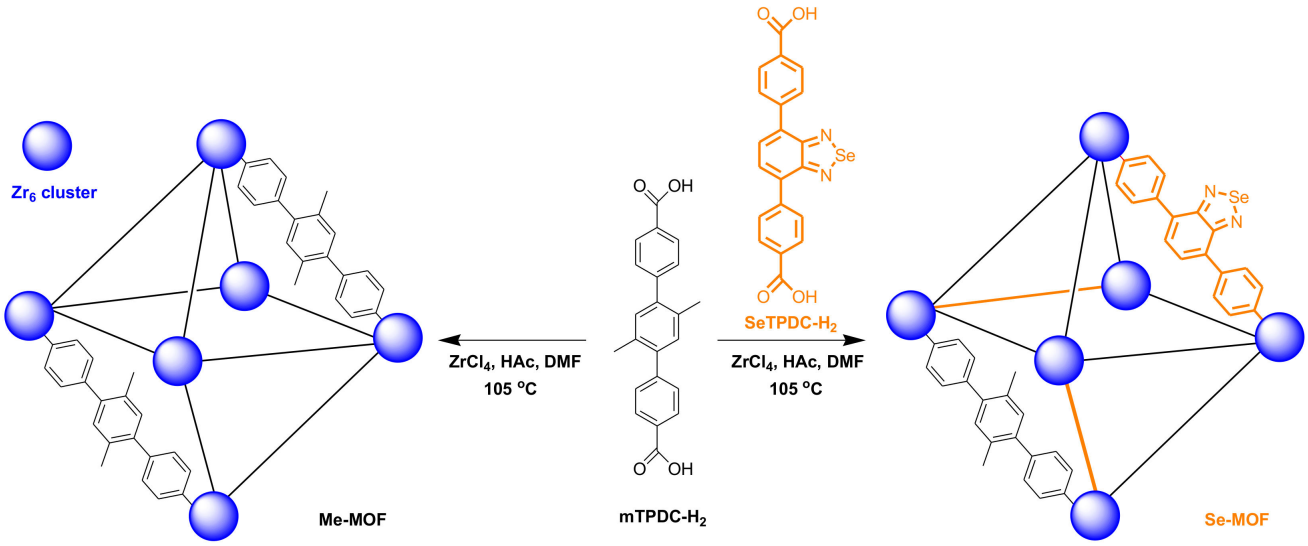

Figure 1. Schematic representation of the preparation for Me-MOF and Se-MOF.

2. Results and Discussion

The synthetic processes of mTPDC-H2 and SeTPDC-H2 are illustrated in the Supplementary Materials (Schemes S1 and S2), and their chemical structure was determined by ^{1}H NMR spectroscopy (Figures S1 and S2). Using acetic acid (HAc) as an additive, the mixture solution of $ZrCl_4$ and mTPDC-H2 in N,N′-dimethylformamide (DMF) was heated at 105 °C for 48 h. The resulting precipitation was collected by centrifugation and washed three times with DMF to give Me-MOF. The morphology of Me-MOF was observed by scanning electron microscopy (SEM). As shown in Figure 2A, Me-MOF has an octahedral morphological structure, and its average diameter is approximately 1.2 μm. Furthermore,

mTPDC-H2 and SeTPDC-H2 were mixed in a mole ratio of 4:1 to prepare the Se-MOF using similar methods. It can be seen in Figure 2B that there was no difference in morphology between Me-MOF and Se-MOF. Furthermore, the porous structure on the surface of the MOF was observed in the enlarged SEM images of both samples.

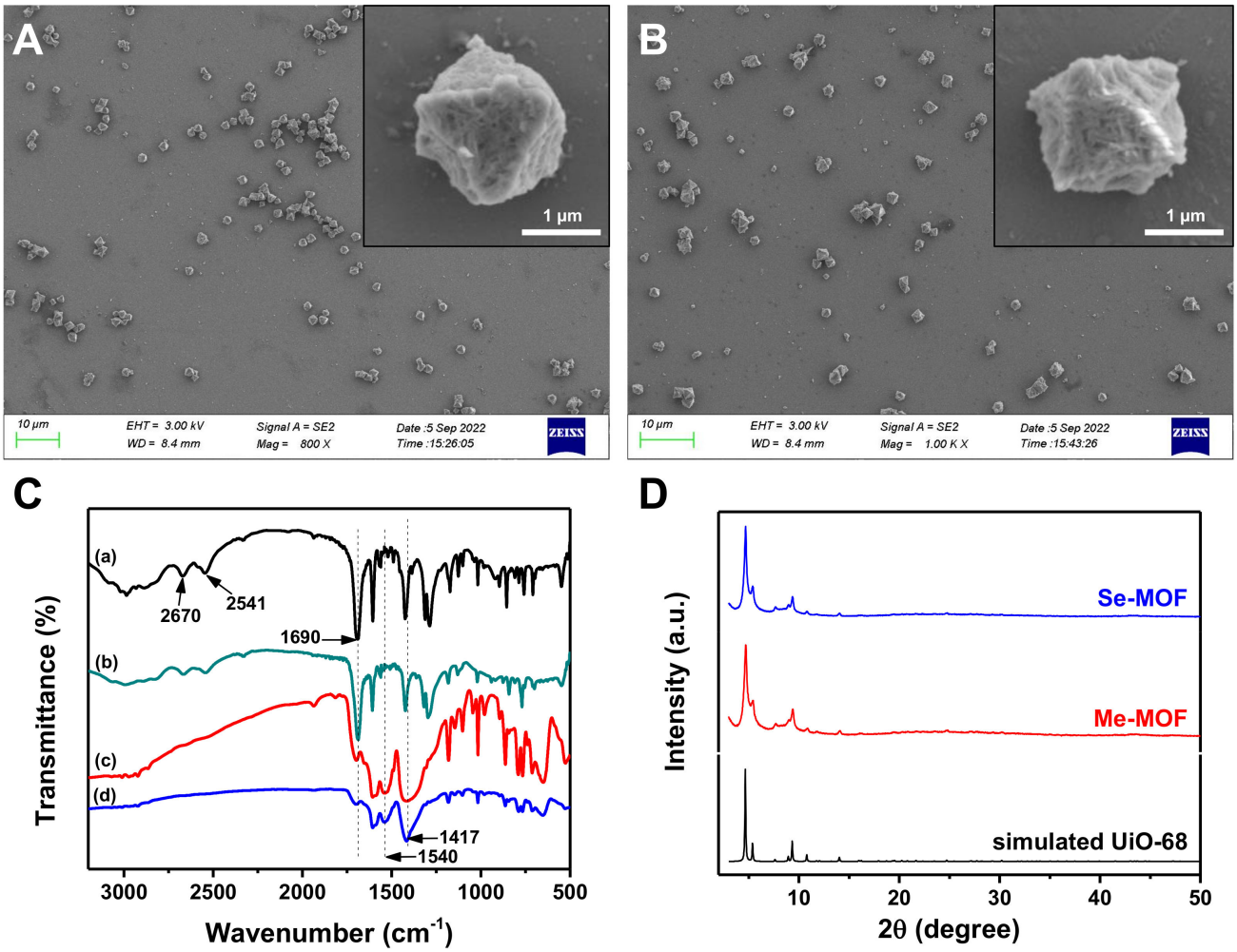

Figure 2. SEM images of (**A**) Me-MOF and (**B**) Se-MOF. (**C**) FT−IR spectra of (a) mTCDP-H2, (b) SeTPDC-H2, (c) Me-MOF, and (d) Se-MOF. (**D**) XRD patterns of the Me-MOF and Se-MOF.

The formation of MOF structure was confirmed using Fourier transform infrared (FT-IR) spectroscopy. The FT-IR spectra of Me-MOF and Se-MOF were measured and compared with those of mTPDC-H2 and SeTPDC-H2 (Figure 2C). For mTPDC-H2 and SeTPDC-H2, there was a characteristic peak at 1690 cm^{-1} due to the stretching vibrations of the carboxyl C=O group. However, the intensity of the peak at 1690 cm^{-1} decreases significantly and two new peaks at 1540 and 1417 cm^{-1} were observed in the FT-IR spectra of Me-MOF and Se-MOF, indicating the formation of a coordination bond between the Zr^{4+} and carboxyl groups [37]. Powder X-ray diffraction (XRD) patterns of Me-MOF and Se-MOF are shown in Figure 2D. Three characteristic peaks at 2θ = 4.54°, 5.24°, and 9.16° were observed for two MOF samples, and their relative intensity was consistent with the simulated pattern from single-crystal data, confirming their regular crystallinity and UiO-68 topological framework [38,39].

The nitrogen adsorption/desorption isotherms were measured to verify the porous feature of the MOFs. As shown in Figure 3A, a typical type I reversible isotherm was observed for the Me-MOF and Se-MOF. According to Brunauer-Emmett-Teller (BET) analysis, Me-MOF and Se-MOF have surface areas of 2991 and 2882 m^2 g^{-1}, respectively. As shown

in Figure 3B, an average pore diameter of ~2 nm was calculated by Barret-Joyner-Halenda (BJH) analysis. Next, two MOF samples were dispersed in DMF, and fluorescence spectra were measured at room temperature. Compared to Me-MOF, Se-MOF has a longer excitation wavelength in the range of 400–475 nm (Figure 3C). Furthermore, the maximum fluorescence emission of Se-MOF was at 523 nm, but no fluorescence was observed for Me-MOF (Figure 3D).

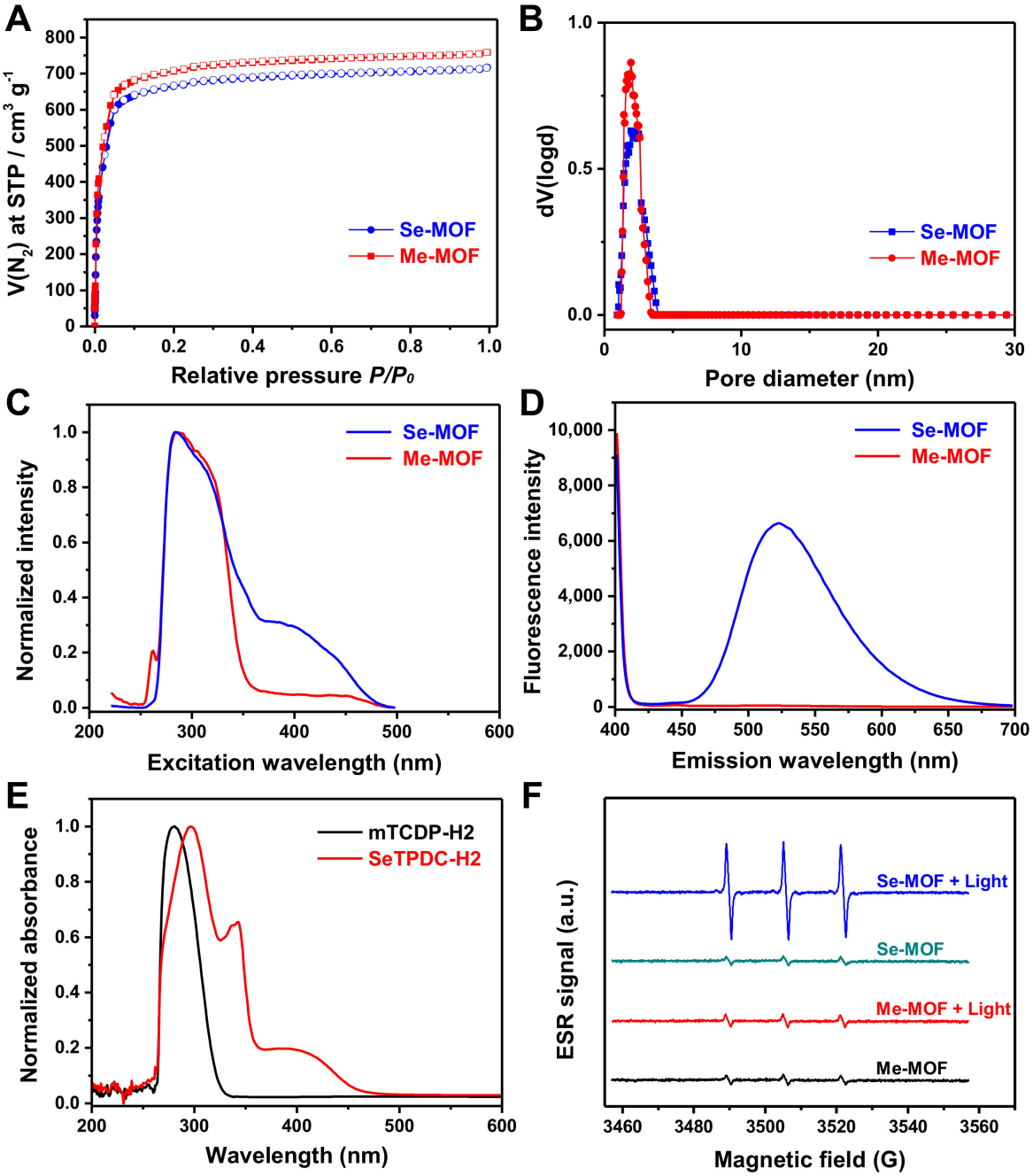

Figure 3. (**A**) Nitrogen sorption isotherms and (**B**) Barrett−Joyner−Halenda pore distribution of the Me-MOF and Se-MOF. (**C**) Excitation spectra (λ_{em} = 522 nm) and (**D**) emission spectra (λ_{ex} = 390 nm) of the Me-MOF and Se-MOF dispersed in DMF. (**E**) UV−vis absorption spectra of mTPDC-H2 and SeTPDC-H2 in DMF. (**F**) ESR spectra of a PBS solution (pH 7.4) containing Me-MOF or Se-MOF before and after light irradiation (450 nm, 3 mW cm^{-2}).

UV-vis absorption spectra of mTPDC-H2 and SeTPDC-H2 in DMF were also recorded (Figure 3E). The results show that SeTPDC-H2 has both UV and visible light absorption (260–470 nm), while mTPDC-H2 only has UV absorption (260–330 nm). Thus, a blue light-emitting diode (LED) lamp (450 nm) was used as the light source to stimulate the photoactivity of Se-MOF in the following experiments. Next, electron spin resonance (ESR) was used to evaluate the efficiency of $^1O_2$ generation for Me-MOF and Se-MOF under 450 nm light irradiation with a density of 3 mW cm^{-2} for 5 min. First, two MOF samples were dispersed in phosphate-buffered saline (PBS) solutions (pH 7.4) at a concentration of 1.0 mg mL^{-1}, and 2,2,6,6-tetramethylpiperidine (TEMP) was used to monitor $^1O_2$ generation before and after irradiation. As shown in Figure 3F, no noticeable change in the ESR signal was observed for Me-MOF after irradiation, which should be attributed to the fact that mTPDC-H2 has no absorption at 450 nm. However, a much stronger characteristic signal of $^1O_2$ was observed in the ESR spectra of Se-MOF under light irradiation. These results show that incorporating SeTPDC-H2 into the MOF skeletons enables Se-MOF to generate $^1O_2$ under 450 nm light irradiation, indicating the application potential of Se-MOF as a photodynamic agent.

The photodynamic antibacterial activity of Me-MOF and Se-MOF against *S. aureus* was evaluated using a two-fold serial dilution method [40–42]. The bacteria were incubated with different concentrations of MOF materials, followed by irradiation with a LED light (450 nm, 3 mW cm^{-2}) for 20 min. After light irradiation was repeated three times, the bacterial suspension was diluted and cultured on Luria-Bertani (LB) agar plates. As shown in the digital photographs (Figure 4A), the number of bacteria was calculated according to ImageJ software and analyzed for comparison. As shown in Figure 4B, the results showed that the photoactivity of Se-MOF was significantly higher than that of Me-MOF under identical conditions. This outcome should be because Se-MOF produced $^1O_2$ under 450 nm light irradiation, thus causing more significant photodamage to bacterial cells. In addition, the dark toxicity of Me-MOF and Se-MOF against *S. aureus* was also studied. In the absence of light, no differences in bacterial viability were observed between Me-MOF and Se-MOF (Figure 4C). Thus, these results further demonstrated the potential of Se-MOF for antibacterial PDT applications.

The bacterial biofilm model was established to investigate the inhibition effect of Se-MOF on biofilm formation under visible light irradiation. Both PBS and Me-MOF were used as control samples. Since Me-MOF has the same physical and chemical properties as Se-MOF, Me-MOF was selected as the control to avoid interference by other factors (controlled release of antibacterial components, sizes, morphologies, surface charges, and interaction with the bacterial cell wall) on bactericidal performance [43,44]. First, *S. aureus* bacteria were incubated in the medium containing Me-MOF or Se-MOF at an equivalent concentration of 50 μg mL^{-1}. After being irradiated three times with a LED light (450 nm, 3 mW cm^{-2}) for 20 min, the bacterial suspension was cultured on 96-well plates. The biofilm inhibition efficiency of Se-MOF at different time points was studied by crystal violet (CV) staining. Representative images of the plate are presented in Figure 5A and the optical density (OD) at 590 nm was measured using a microplate reader. The data indicated that Me-MOF has no inhibition effect on the biofilms of bacteria under 450 nm light irradiation. However, Se-MOF significantly inhibited the formation of bacteria biofilms under identical conditions. As the $^1O_2$ produced by Se-MOF inhibited bacterial reproduction, it destroyed bacterial aggregation to form biofilms. Therefore, these results confirmed that Se-MOF could be used as photosensitive MOFs for the photodynamic killing of bacteria and inhibition of biofilm formation.

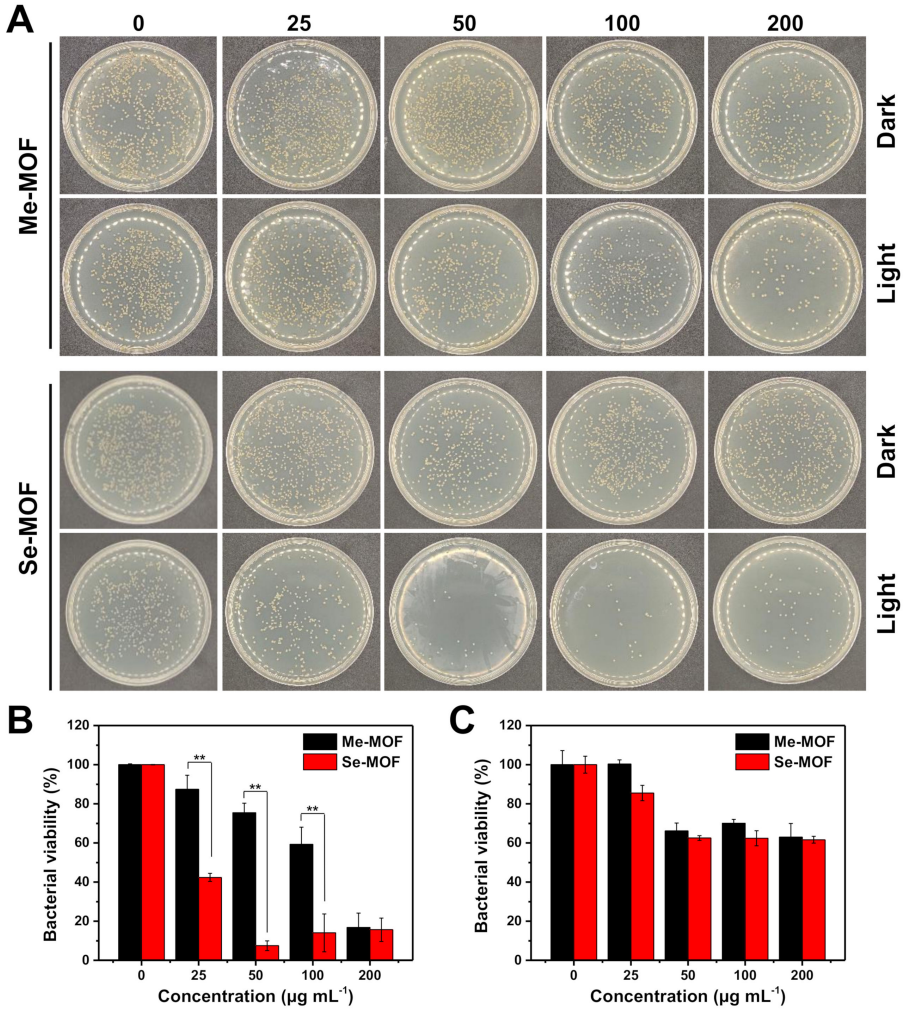

Figure 4. (**A**) Representative photographs of *S. aureus* colonies in LB agar plates after being incubated with different concentrations of Me-MOF or Se-MOF, followed by irradiation three times with a LED light (450 nm, 3 mW cm^{-2}) for 20 min or incubation in the dark. (**B**,**C**) Percentage viability of bacteria *S. aureus* after different treatments, followed by light irradiation (**B**) or incubation in the dark (**C**). Data are presented as mean ± standard deviation (n = 3; ** $p < 0.01$).

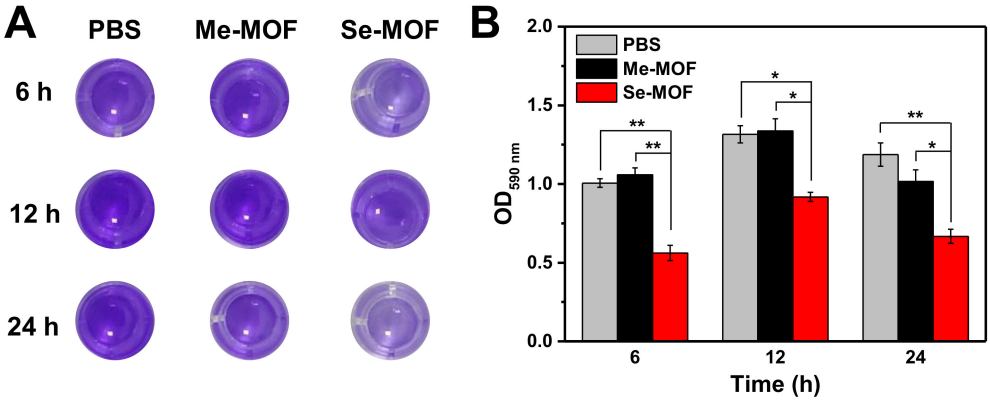

Figure 5. (**A**) Representative photographs of CV−stained biofilms after being incubated with Me-MOF or Se-MOF, followed by irradiation three times with LED light (450 nm, 3 mW cm^{-2}) for 20 min. (**B**) Quantification of the OD measurement from the CV−stained biofilms in (**A**). Data are presented as mean ± standard deviation (n = 3; * $p < 0.05$ and ** $p < 0.01$).

3. Materials and Methods

3.1. Synthesis of mTPDC-H2 and SeTPDC-H2

The synthesis procedures are described in the Supplementary Materials.

3.2. Preparation of Me-MOF

mTPDC-H2 (200 mg, 0.58 mmol) was dissolved in DMF (100 mL), and then $ZrCl_4$ (150 mg, 0.64 mmol) and acetic acid (3 mL, 0.05 mmol) were added to the solution. The mixture was heated to 105 °C and stirred for 48 h. Then, the crude product was collected by centrifugation and washed three times with DMF (100 mL) and ethanol (100 mL), respectively. Finally, the sample was dried under reduced pressure and denoted as Me-MOF.

3.3. Preparation of Se-MOF

mTPDC-H2 (140 mg, 0.4 mmol) and SeTPDC-H2 (44 mg, 0.1 mmol) were dissolved in DMF (100 mL). After adding $ZrCl_4$ (120 mg, 0.51 mmol) and acetic acid (3 mL, 0.05 mmol) to the solution, the mixture was heated to 105 °C and stirred for 48 h. Then, the crude product was collected by centrifugation and washed three times with DMF (100 mL) and ethanol (100 mL), respectively. Finally, the sample was dried under reduced pressure and denoted as Se-MOF.

3.4. Antibacterial Assay

Monoclonal colonies of *S. aureus* grown in the LB agar plate were transferred to an LB culture medium (10 mL) and grown at 37 °C for 12 h. After the bacterial suspension was diluted to 10^5 CFU/mL (OD_{600nm} = 0.001), 100 μL of the diluted bacterial suspension was incubated with different concentrations of Me-MOF or Se-MOF in a 96-well plate. The plate was irradiated with a blue LED light (450 nm, 3 mW cm^{-2}) for 20 min, and the irradiation was repeated three times. After the bacteria were further incubated at 37 °C for 12 h, the bacterial solution was diluted 10^{-5} times and 100 μL of the diluted bacterial solution was streaked on LB agar plates using the spread plate method. After the plates were cultured for 12 h, the number of colony-forming units was counted by ImageJ software.

3.5. CV Staining of Bacteria Biofilms

The bacterial suspension was diluted to 10^7 CFU/mL (OD_{600nm} = 0.1), and 100 μL of the diluted bacterial suspension was incubated with Me-MOF or Se-MOF at an equivalent concentration of 50 μg mL^{-1} in a 96-well plate. The plate was irradiated with a blue LED light (450 nm, 3 mW cm^{-2}) for 20 min, and the irradiation was repeated three times. At different times of incubation (6, 12, and 24 h), the biofilms were observed and quantified using a CV staining method [45–47]. The biofilms were fixed with 4.0% paraformaldehyde and then stained with an aqueous CV solution (0.1% w/v) for 30 min. After removal of the CV solution, the stained biofilms were washed three times with PBS (pH 7.4) and then dissolved in an ethanol solution (95% v/v). Finally, the optical density at 590 nm (OD_{590nm}) was measured using a microplate reader (Varioskan LUX, ThermoFisher SCIENTIFIC, Waltham, MA, USA) to determine biofilm biomass.

4. Conclusions

In summary, we have synthesized Se-MOF as an antibacterial material for the photodynamic inactivation of bacteria and biofilms. The obtained Se-MOF is a topological UiO-68 framework with a diameter of ~1.2 μm. The results demonstrated that incorporating benzoselenadiazole-containing ligands into MOF skeletons endowed them with high efficiency to produce $^1O_2$ under 450 nm light irradiation, causing photodynamic inactivation of *S. aureus* bacteria. In particular, Se-MOF could efficiently inhibit the formation of bacterial biofilms upon visible-light irradiation. Thus, Se-MOF may be promising MOF-based PDT agents for the photodynamic killing of bacteria and inhibition of biofilm formation.

Supplementary Materials: The following supporting information can be downloaded at: https://www.mdpi.com/article/10.3390/molecules27248908/s1, Experimental details for the synthesis of mTPDC-H2 and SeTPDC-H2; Schemes S1 and S2: synthetic route of mTPDC-H2 and SeTPDC-H2; Figures S1 and S2: 1H NMR and ^{13}C NMR spectra of mTPDC-H2; Figures S3 and S4: 1H NMR and 13C NMR spectra of SeTPDC-H2.

Author Contributions: Conceptualization, Q.Z.; Data curation, L.L. and L.D.; Funding acquisition, Y.L.; Investigation, L.L., L.D. and W.S.; Methodology, L.L. and L.D.; Supervision, Y.L. and Q.Z.; writing—original draft, L.L. and L.D.; Writing—review and editing, Q.Z. All authors have read and agreed to the published version of the manuscript.

Funding: This research was funded by the Liaoning Natural Science Foundation (Grant 2021-MS-046) and the Science and Technology Program of Liaoning Province (Grant 2020JH2/10300098).

Institutional Review Board Statement: Not applicable.

Informed Consent Statement: Not applicable.

Data Availability Statement: Not applicable.

Acknowledgments: This research was financially supported by the Liaoning Natural Science Foundation (Grant 2021-MS-046) and the Science and Technology Program of Liaoning Province (Grant 2020JH2/10300098). We thank Professor Xiaojun Wang at Jiangsu Normal University for his advice and discussions.

Conflicts of Interest: The authors declare no conflict of interest.

Sample Availability: Samples of the compounds are available from the authors.

References

1. Laxminarayan, R.; Duse, A.; Wattal, C.; Zaidi, A.K.; Wertheim, H.F.; Sumpradit, N.; Vlieghe, E.; Hara, G.L.; Gould, I.M.; Goossens, H.; et al. Antibiotic Resistance-the Need for Global Solutions. *Lancet Infect. Dis.* **2013**, *13*, 1057–1098. [CrossRef] [PubMed]
2. Antimicrobial Resistance Collaborators. Global Burden of Bacterial Antimicrobial Resistance in 2019: A Systematic Analysis. *Lancet* **2022**, *399*, 629–655. [CrossRef] [PubMed]
3. Pulingam, T.; Parumasivam, T.; Gazzali, A.M.; Sulaiman, A.M.; Chee, J.Y.; Lakshmanan, M.; Chin, C.F.; Sudesh, K. Antimicrobial Resistance: Prevalence, Economic Burden, Mechanisms of Resistance and Strategies to Overcome. *J. Pharm. Sci.* **2022**, *170*, 106103. [CrossRef] [PubMed]
4. Roy, R.; Tiwari, M.; Donelli, G.; Tiwari, V. Strategies for Combating Bacterial Biofilms: A Focus on Anti-biofilm Agents and Their Mechanisms of Action. *Virulence* **2018**, *9*, 522–554. [CrossRef]
5. Ćirić, A.D.; Petrović, J.D.; Glamočlija, J.M.; Smiljković, M.S.; Nikolić, M.M.; Stojković, D.S.; Soković, M.D. Natural Products as Biofilm Formation Antagonists and Negulators of Quorum Sensing Functions: A Comprehensive Review Update and Future Trends. *S. Afr. J. Bot.* **2019**, *120*, 65–80. [CrossRef]
6. Kalelkar, P.P.; Riddick, M.; Garcia, A.J. Biomaterial-Based Antimicrobial Therapies for The Treatment of Bacterial Infections. *Nat. Rev. Mater.* **2022**, *7*, 39–54. [CrossRef]
7. Vinagreiro, C.S.; Zangirolami, A.; Schaberle, F.A.; Nunes, S.C.C.; Blanco, K.C.; Inada, N.M.; da Silva, G.J.; Pais, A.; Bagnato, V.S.; Arnaut, L.G.; et al. Antibacterial Photodynamic Inactivation of Antibiotic-Resistant Bacteria and Biofilms with Nanomolar Photosensitizer Concentrations. *ACS Infect. Dis.* **2020**, *6*, 1517–1526. [CrossRef]
8. Cao, Y.; Naseri, M.; He, Y.; Xu, C.; Walsh, L.J.; Ziora, Z.M. Non-Antibiotic Antimicrobial Agents to Combat Biofilm-Forming Bacteria. *J. Glob. Antimicrob. Resist.* **2020**, *21*, 445–451. [CrossRef]
9. Hemmati, F.; Rezaee, M.A.; Ebrahimzadeh, S.; Yousefi, L.; Nouri, R.; Kafil, H.S.; Gholizadeh, P. Novel Strategies to Combat Bacterial Biofilms. *Mol. Biotechnol.* **2021**, *63*, 569–586. [CrossRef]
10. Makabenta, J.M.V.; Nabawy, A.; Li, C.H.; Schmidt-Malan, S.; Patel, R.; Rotello, V.M. Nanomaterial-Based Therapeutics for Antibiotic-Resistant Bacterial Infections. *Nat. Rev. Microbiol.* **2021**, *19*, 23–36. [CrossRef]
11. Dai, X.; Zhang, B.; Yu, Q.; Liu, Y. Multicharged Supramolecular Assembly Mediated by Polycationic Cyclodextrin for Efficiently Photodynamic Antibacteria. *ACS Appl. Bio Mater.* **2021**, *4*, 8536–8542. [CrossRef] [PubMed]
12. Songca, S.P.; Adjei, Y. Applications of Antimicrobial Photodynamic Therapy against Bacterial Biofilms. *Int. J. Mol. Sci.* **2022**, *23*, 3209. [CrossRef] [PubMed]
13. Hamblin, M.R. Antimicrobial Photodynamic Inactivation: A Bright New Technique to Kill Resistant Microbes. *Curr. Opin. Microbiol.* **2016**, *33*, 67–73. [CrossRef] [PubMed]

14. Seeger, M.G.; Ries, A.S.; Gressler, L.T.; Botton, S.A.; Iglesias, B.A.; Cargnelutti, J.F. In Vitro Antimicrobial Photodynamic Therapy Using Tetra-Cationic Porphyrins Against Multidrug-Resistant Bacteria Isolated from Canine Otitis. *Photodiagnosis Photodyn. Ther.* **2020**, *32*, 101982. [CrossRef] [PubMed]
15. Ding, L.-G.; Wang, S.; Yao, B.-J.; Li, F.; Li, Y.-A.; Zhao, G.-Y.; Dong, Y.-B. Synergistic Antibacterial and Anti-Inflammatory Effects of a Drug-Loaded Self-Standing Porphyrin-COF Membrane for Efficient Skin Wound Healing. *Adv. Healthc. Mater.* **2021**, *10*, 2001821. [CrossRef]
16. Galstyan, A. Turning Photons into Drugs: Phthalocyanine-Based Photosensitizers as Efficient Photoantimicrobials. *Chemistry* **2021**, *27*, 1903–1920. [CrossRef]
17. Gunsel, A.; Taslimi, P.; Atmaca, G.Y.; Bilgicli, A.T.; Piskin, H.; Ceylan, Y.; Erdogmus, A.; Yarasir, M.N.; Gulcin, I. Novel Potential Metabolic Enzymes Inhibitor, Photosensitizer and Antibacterial Agents Based on Water-Soluble Phthalocyanine Bearing Imidazole Derivative. *J. Mol. Struct.* **2021**, *1237*, 130402. [CrossRef]
18. Zhang, Y.; Zhao, R.; Liu, J.; Kong, H.; Zhang, K.; Zhang, Y.-N.; Kong, X.; Zhang, Q.; Zhao, Y. Hierarchical Nano-to-Molecular Disassembly of Boron Dipyrromethene Nanoparticles for Enhanced Tumor Penetration and Activatable Photodynamic Therapy. *Biomaterials* **2021**, *275*, 120945. [CrossRef]
19. Cao, J.; Zhang, Y.; Shi, W.; Du, L.; Cui, Z.; Liu, S.; Zhao, R.; Wang, S.; Zhang, Q.; Kong, X. Mitochondria-Targeted Photodynamic Cancer Therapy of Nanoscale Liposome-Encapsulating Boron Dipyrromethene Photosensitizers Conjugated with Pyridine Cations. *ACS Appl. Nano Mater.* **2022**, *5*, 5459–5469. [CrossRef]
20. Shi, X.; Sung, S.H.P.; Chau, J.H.C.; Li, Y.; Liu, Z.; Kwok, R.T.K.; Liu, J.; Xiao, P.; Zhang, J.; Liu, B.; et al. Killing G(+) or G(−) Bacteria? The Important Role of Molecular Charge in AIE-Active Photosensitizers. *Small Methods* **2020**, *4*, 2000046. [CrossRef]
21. Chen, J.; Fan, T.; Xie, Z.; Zeng, Q.; Xue, P.; Zheng, T.; Chen, Y.; Luo, X.; Zhang, H. Advances in Nanomaterials for Photodynamic Therapy Applications: Status and Challenges. *Biomaterials* **2020**, *237*, 119827. [CrossRef] [PubMed]
22. Zhao, X.; Liu, J.; Fan, J.; Chao, H.; Peng, X. Recent Progress in Photosensitizers for Overcoming the Challenges of Photodynamic Therapy: From Molecular Design to Application. *Chem. Soc. Rev.* **2021**, *50*, 4185–4219. [CrossRef] [PubMed]
23. Zhang, Y.; Wang, B.; Zhao, R.; Zhang, Q.; Kong, X. Multifunctional Nanoparticles as Photosensitizer Delivery Carriers for Enhanced Photodynamic Cancer Therapy. *Mater. Sci. Eng. C* **2020**, *115*, 111099. [CrossRef] [PubMed]
24. Ziental, D.; Czarczynska-Goslinska, B.; Mlynarczyk, D.T.; Glowacka-Sobotta, A.; Stanisz, B.; Goslinski, T.; Sobotta, L. Titanium Dioxide Nanoparticles: Prospects and Applications in Medicine. *Nanomaterials* **2020**, *10*, 387. [CrossRef] [PubMed]
25. Jiao, H.-F.; Guo, J.; Cui, Y.; Yu, X.; Liao, Y.; Ying, Y.; Li, Z.; Yao, K.; Huang, H. Plasmon-Enhanced Photocatalytic Activity of Organic Heterostructure for Indoor-Light Antibacterial Therapy. *Adv. Ther.* **2022**, *5*, 2100202. [CrossRef]
26. Wang, L.; Zhang, X.; Yu, X.; Gao, F.; Shen, Z.; Zhang, X.; Ge, S.; Liu, J.; Gu, Z.; Chen, C. An All-Organic Semiconductor C3N4/PDINH Heterostructure with Advanced Antibacterial Photocatalytic Therapy Activity. *Adv. Mater.* **2019**, *31*, 1901965. [CrossRef]
27. Wei, Y.-S.; Zhang, M.; Zou, R.; Xu, Q. Metal-Organic Framework-Based Catalysts with Single Metal Sites. *Chem. Rev.* **2020**, *120*, 12089–12174. [CrossRef]
28. Cheng, W.; Tang, X.; Zhang, Y.; Wu, D.; Yang, W. Applications of Metal-Organic Framework (MOF)-based Sensors for Food Safety: Enhancing Mechanisms and Recent Advances. *Trends Food Sci. Technol.* **2021**, *112*, 268–282. [CrossRef]
29. Kung, C.-W.; Goswami, S.; Hod, I.; Wang, T.C.; Duan, J.; Farha, O.K.; Hupp, J.T. Charge Transport in Zirconium-Based Metal-Organic Frameworks. *Acc. Chem. Res.* **2020**, *53*, 1187–1195. [CrossRef]
30. Mao, D.; Hu, F.; Kenry; Ji, S.; Wu, W.; Ding, D.; Kong, D.; Liu, B. Metal-Organic-Framework-Assisted in Vivo Bacterial Metabolic Labeling and Precise Antibacterial Therapy. *Adv. Mater.* **2018**, *30*, 1706831. [CrossRef]
31. Simon-Yarza, T.; Mielcarek, A.; Couvreur, P.; Serre, C. Nanoparticles of Metal-Organic Frameworks: On the Road to in Vivo Efficacy in Biomedicine. *Adv. Mater.* **2018**, *30*, 1707365. [CrossRef] [PubMed]
32. Sun, Y.; Zheng, L.; Yang, Y.; Qian, X.; Fu, T.; Li, X.; Yang, Z.; Yan, H.; Cui, C.; Tan, W. Metal-Organic Framework Nanocarriers for Drug Delivery in Biomedical Applications. *Nano-Micro Lett.* **2020**, *12*, 103. [CrossRef] [PubMed]
33. Zheng, Q.; Liu, X.; Zheng, Y.; Yeung, K.W.K.; Cui, Z.; Liang, Y.; Li, Z.; Zhu, S.; Wang, X.; Wu, S. The Recent Progress on Metal-Organic Frameworks for Phototherapy. *Chem. Soc. Rev.* **2021**, *50*, 5086–5125. [CrossRef] [PubMed]
34. Schlachter, A.; Asselin, P.; Harvey, P.D. Porphyrin-Containing MOFs and COFs as Heterogeneous Photosensitizers for Singlet Oxygen-Based Antimicrobial Nanodevices. *ACS Appl. Mater. Interfaces* **2021**, *13*, 26651–26672. [CrossRef]
35. Mao, K.; Zhu, Y.; Rong, J.; Qiu, F.; Chen, H.; Xu, J.; Yang, D.; Zhang, T.; Zhong, L. Rugby-Ball Like Ag Modified Zirconium Porphyrin Metal-Organic Frameworks Nanohybrid for Antimicrobial Activity: Synergistic Effect for Significantly Enhancing Photoactivation Capacity. *Colloids Surf. A* **2021**, *611*, 125888. [CrossRef]
36. Zhang, W.-Q.; Li, Q.-Y.; Zhang, Q.; Lu, Y.; Lu, H.; Wang, W.; Zhao, X.; Wang, X.-J. Robust Metal-Organic Framework Containing Benzoselenadiazole for Highly Efficient Aerobic Cross-dehydrogenative Coupling Reactions under Visible Light. *Inorg. Chem.* **2016**, *55*, 1005–1007. [CrossRef]
37. Mostakim, S.K.; Biswas, S. A Thiadiazole-Functionalized Zr(IV)-Based Metal–Organic Framework as a Highly Fluorescent Probe for the Selective Detection of Picric Acid. *CrystEngComm* **2016**, *18*, 3104–3113. [CrossRef]
38. Ye, X.; Liu, D. Metal–Organic Framework UiO-68 and Its Derivatives with Sufficiently Good Properties and Performance Show Promising Prospects in Potential Industrial Applications. *Cryst. Growth Des.* **2021**, *21*, 4780–4804. [CrossRef]

39. Wu, S.; Ren, D.; Zhou, K.; Xia, H.-L.; Liu, X.-Y.; Wang, X.; Li, J. Linker Engineering toward Full-Color Emission of UiO-68 Type Metal-Organic Frameworks. *J. Am. Chem. Soc.* **2021**, *143*, 10547–10552. [CrossRef]
40. Li, P.; Ruan, L.; Jiang, G.; Sun, Y.; Wang, R.; Gao, X.; Yunusov, K.E.; Aharodnikau, U.E.; Solomevich, S.O. Design of 3D Polycaprolactone/ε-Polylysine-Modified Chitosan Fibrous Scaffolds with Incorporation of Bioactive Factors for Accelerating Wound Healing. *Acta Biomater.* **2022**, *152*, 197–209. [CrossRef]
41. Yang, Y.; Li, M.; Zhou, C.; Zhou, K.; Yu, J.; Su, Y.; Hu, N.; Zhang, Y. Laser-Induced MoOx/Sulfur-Doped Graphene Hybrid Frameworks as Efficient Antibacterial Agents. *Langmuir* **2021**, *37*, 1596–1604. [CrossRef]
42. Deng, Q.; Sun, P.; Zhang, L.; Liu, Z.; Wang, H.; Ren, J.; Qu, X. Porphyrin MOF Dots–Based, Function-Adaptive Nanoplatform for Enhanced Penetration and Photodynamic Eradication of Bacterial Biofilms. *Adv. Funct. Mater.* **2019**, *29*, 1903018. [CrossRef]
43. Li, R.; Chen, T.; Pan, X. Metal-Organic-Framework-Based Materials for Antimicrobial Applications. *ACS Nano* **2021**, *15*, 3808–3848. [CrossRef] [PubMed]
44. Polash, S.A.; Khare, T.; Kumar, V.; Shukla, R. Prospects of Exploring the Metal-Organic Framework for Combating Antimicrobial Resistance. *ACS Appl. Bio Mater.* **2021**, *4*, 8060–8079. [CrossRef] [PubMed]
45. Ding, M.; Zhao, W.; Zhang, X.; Song, L.; Luan, S. Charge-Switchable MOF Nanocomplex for Enhanced Biofilm Penetration and Eradication. *J. Hazard. Mater.* **2022**, *439*, 129594. [CrossRef] [PubMed]
46. Narayanan, K.B.; Kim, H.D.; Han, S.S. Biocompatibility and Hemocompatibility of Hydrothermally Derived Reduced Graphene Oxide Using Soluble Starch as a Reducing Agent. *Colloids Surf. B* **2020**, *185*, 110579. [CrossRef] [PubMed]
47. Shi, Y.; Cao, Y.; Cheng, J.; Yu, W.; Liu, M.; Yin, J.; Huang, C.; Liang, X.; Zhou, H.; Liu, H.; et al. Construction of Self-Activated Nanoreactors for Cascade Catalytic Anti-Biofilm Therapy Based on H_2O_2 Self-Generation and Switch-On NO Release. *Adv. Funct. Mater.* **2022**, *32*, 2111148. [CrossRef]